ACS POLYMERS Au
AN OPEN ACCESS JOURNAL OF THE AMERICAN CHEMICAL SOCIETY

pubs.acs.org/polymerau

Article

Photolithographic Fabrication of Mechanically Adaptive Devices

Baptiste Monney, Cédric Kilchoer, and Christoph Weder*

Cite This: *ACS Polym. Au* 2022, 2, 50–58

Read Online

ACCESS | Metrics & More | Article Recommendations | Supporting Information

ABSTRACT: Water-responsive polymers, which enable the design of objects whose mechanical properties or shape can be altered upon moderate swelling, are useful for a broad range of applications. However, the limited processing options of materials that exhibit useful switchable mechanical properties generally restricted their application to objects having a simple geometry. Here we show that this problem can be overcome by using a negative photoresist approach in which a linear hydrophilic polymer is converted into a highly transparent cross-linked polymer network. The photolithographic process allows the facile production of objects of complex shape and permits programming of the cross-link density, the extent of aqueous swelling, and thereby the stiffness and refractive index under physiological conditions over a wide range and with high spatial resolution. Our findings validate a straightforward route to fabricate mechanically adaptive devices for a variety of (biomedical) uses, notably optogenetic implants whose overall shape, mechanical contrast, and optical channels can all be defined by photolithography.

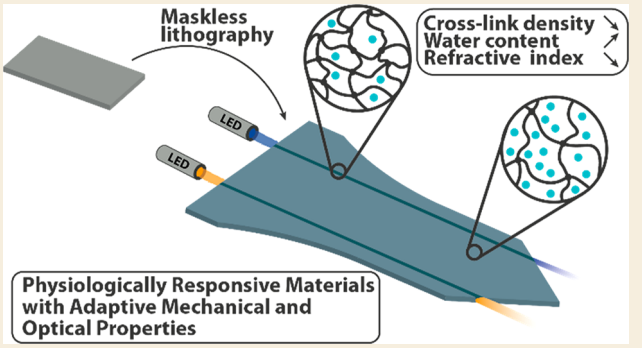

KEYWORDS: *Mechanically adaptive, water-responsive, polymer, photolithography, photoresist, switchable properties, optogenetic, implant, waveguide*

INTRODUCTION

Materials systems that enable the fabrication of objects whose mechanical properties and/or shape can be controlled by a stimulus are omnipresent in living organisms, and considerable efforts have been made to realize such responses in synthetic polymers.[1] Water-responsive polymers that offer large property changes upon swelling represent a subset of this class of materials.[2] Their properties are, for example, useful to create actuators,[3] sensors,[4] adaptive membranes,[5] and biomedical devices or implants that soften upon exposure to physiological conditions.[6,7] The latter concept has been used to devise adaptive neural implants, including cortical electrodes and optical probes.[8,9] Such devices are useful to treat a range of medical conditions,[10−16] but the long-term functionality of rigid cortical implants was shown to be impacted by the mechanical mismatch with the soft cortical tissue.[17−19] This problem can be mitigated by devices that are initially rigid and allow facile implantation but soften when exposed to physiological conditions.[20−23] Several materials have been developed for this purpose,[1] including nanocomposites of polymers and cellulose nanocrystals, photopolymerizable poly(acrylate)s and poly(methacrylate)s, as well as thiol−ene-based shape-memory polymers.[24−29] These materials all change their stiffness upon water sorption by up to 3 orders of magnitude, which causes plasticization and in the case of nanocomposites also disassembly of the reinforcing hydrogen-bonded cellulose nanocrystal network. Improved neural integration of adaptive implants has been reported in several studies, but limited processing options have restricted the application of water-responsive polymers to simple device geometries and structures and stifled their exploitation in more intricate or complex devices, which are usually fabricated by microelectromechanical systems technology processes.[30,31]

Here we report the processing of a water-responsive, mechanically adaptive polymer by a negative photoresist approach in which a linear hydrophilic polymer is converted into a highly transparent cross-linked polymer network.[27] The photolithographic process allows the facile production of objects of complex shape and permits programming of the cross-link density, the extent of aqueous swelling, and thereby the stiffness and refractive index under physiological conditions over a wide range and with high spatial resolution. Our findings validate a straightforward route to fabricate mechanically adaptive devices for a variety of (biomedical) uses, notably optogenetic implants whose overall shape, mechanical contrast, and optical channels can all be defined by photolithography.

Received: September 22, 2021
Revised: October 25, 2021
Accepted: October 26, 2021
Published: November 8, 2021

https://doi.org/10.1021/acspolymersau.1c00037
ACS Polym. Au 2022, 2, 50–58

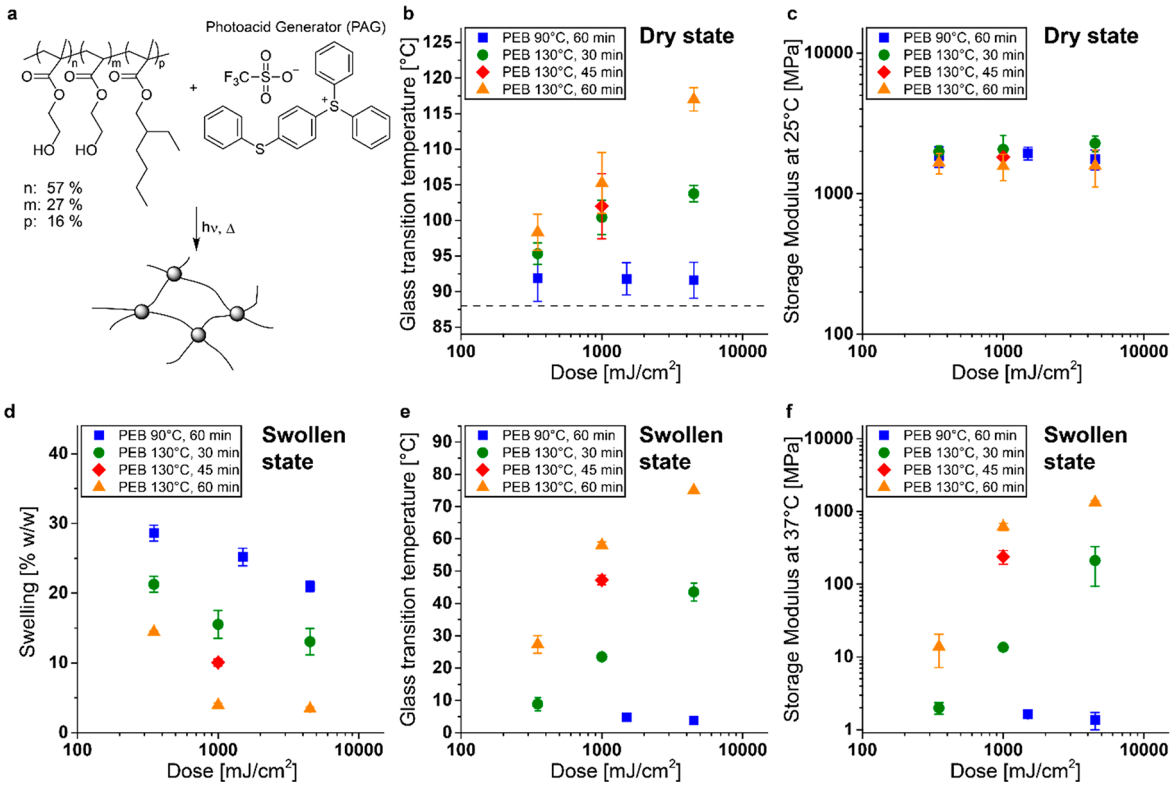

Figure 1. Relationship between process parameters and materials properties. (a) Chemical structure of the parent photoresist used to create the adaptive networks. (b–f) Properties of materials processed by exposure of 100–250 μm thick photoresist films with different doses of 365 nm UV light, curing at different temperatures and times, and subsequent developing. (b) Glass transition temperature (T_g) of dry samples; the dashed line denotes the T_g of the photoresist. (c) Storage modulus (E') at 25 °C of dry samples. (d) Swelling of the materials in ACSF at 37 °C. (e) T_g of samples after swelling in ACSF (overnight, 37 °C). (f) E' at 37 °C of the materials swollen in ACSF. Reported values are the mean ± SD of n = 3 measurements from different samples.

RESULTS AND DISCUSSION

Figure 1a shows the chemical structure of the terpolymer poly(2-hydroxyethyl methacrylate-*co*-2-hydroxyethyl acrylate-*co*-2-ethylhexyl methacrylate) that was combined with 0.5 wt % of the i-line photoacid generator (PAG) (4-phenylthiophenyl)-diphenylsulfonium triflate to form the negative photoresist from which the adaptive materials investigated here were produced.[27] The general cross-linking chemistry employed (vide infra) is well established and has been reported elsewhere.[32−35] The photolithographic fabrication process applied involves processing of the photoresist into films, exposing portions of these films to UV light to locally decompose the PAG, postexposure baking (PEB) to cross-link the polymer in the exposed areas through acid-catalyzed transesterification reactions of the pendant hydroxyl and methacrylate ester groups, and development in appropriate solvents that dissolve the unexposed parts and the PAG residues. In order to explore the relationship between the process parameters and properties, we systematically varied the exposure dose, the PEB temperature, and the PEB duration and analyzed the thermomechanical properties of the materials made in the dry state and, with biomedical applications in mind, under simulated physiological conditions, that is, after equilibration in artificial cerebrospinal fluid (ACSF) at 37 °C. Thus, homogeneous 100–250 μm thick free-standing films of the photoresist were fabricated by solvent casting and cut into rectangular strips (ca. 5 mm × 15 mm). These were exposed in a UV chamber to 365 nm light with a dose of 350–4500 mJ/cm^2, postexposure baked for 30–60 min at 90 or 130 °C, and finally developed in methanol/water mixtures; this protocol was used for all samples studied here.[27]

The examination of dynamic mechanical analysis (DMA) temperature sweeps (Figures S1 and S2) reveals that, in samples produced with a PEB temperature of 90 °C, neither the glass transition temperature (T_g = 92 °C, Figure 1b) nor the storage modulus (E' = 1760–1940 MPa, Figure 1c) in the dry state is substantially affected by the exposure dose, consistent with the fact that the curing temperature is close to the T_g of the photoresist (87 °C, Figure S3). As a result, the low molecular mobility under the curing conditions, and not the UV dose, which determines the amount of acid catalyst released, limit the curing reaction, cross-link density, and thus the T_g. In samples produced with a PEB temperature of 130 °C, the T_g in the dry state varied from 95 to 117 °C and increased with the exposure dose and the PEB duration (Figure 1b), indicating that both parameters influence the cross-link density as expected. In the dry state, all materials exhibit a similar E' value of ca. 1.8 GPa at 25 °C (Figure 1c), reflecting that far below T_g the mechanical properties of these glassy networks are minimally affected by the cross-link density.[36] By contrast, swelling experiments in ACSF at 37 °C (Figure 1d) and DMA analyses of samples equilibrated in ACSF (Figures 1e,f and S2) show clearly that the processing conditions have a very significant influence on the extent of swelling (3–21% w/w, Figure 1d), the T_g after ACSF exposure (9–73 °C, Figure 1e), and the E' under emulated physiological conditions (2–1640 MPa, Figure 1f). The data show the expected dependencies: the T_g and E' increase with increasing

https://doi.org/10.1021/acspolymersau.1c00037
ACS Polym. Au 2022, 2, 50–58

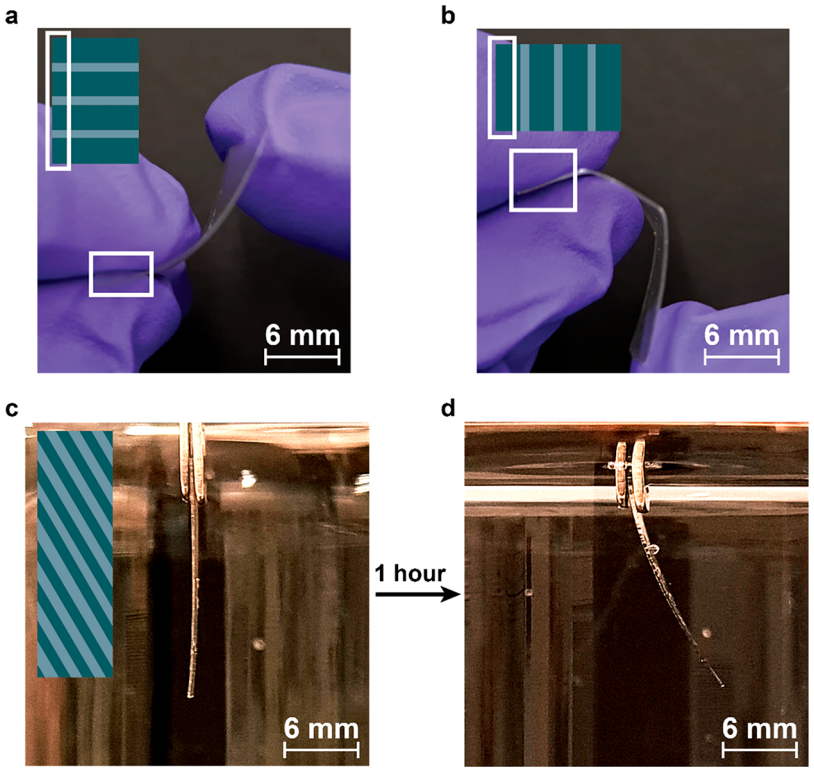

Figure 2. Stimuli-responsive, functionally graded objects fabricated by photolithography. (a, b) Pictures showing the bending characteristics of a crease-containing film perpendicular (a) and parallel (b) to the creases. The inset shows a schematic of the film; the white rectangles indicate where the film is held, and the dark and light blue shades indicate areas of high and low modulus. The film was immersed in ACSF at 37 °C for >2 h prior to testing. The bending was performed at 25 °C. Processing conditions: UV chamber, 365 nm, 350 mJ/cm^2 (light blue) or 4500 mJ/cm^2 (dark blue). PEB: 130 °C, 60 min. (c, d) Pictures showing the action of a previously dry actuator upon immersion in ACSF (at 37 °C) after 0 min (c) and 1 h (d). The inset represents the design of the actuator. Processing conditions: exposition with maskless aligner, 365 nm, 6000 mJ/cm^2 (light blue), 16 000 mJ/cm^2 (dark blue = high exposure dose). PEB: 130 °C, 30 min. The dimensions of the designs are available in Figures S6 and S9.

exposure dose, PEB temperature, and PEB time, that is, with increasing cross-link density, while the extent of swelling decreases.

Having demonstrated that the variation of the process parameters allows the production of mechanically adaptive materials with a dry E' of 1.8 GPa that drops under (emulated) physiological conditions to a value that can be programmed between 1.6 GPa and 2 MPa with only moderate swelling, we applied the process to create stimuli-responsive, functionally graded objects. As a first proof of concept, we fabricated an object with latent creases, which *under physiological conditions* can serve as hinges and impart anisotropic foldability, akin to complex biological materials that connect hard and soft tissues.[37,38] This was achieved by first homogeneously exposing a photoresist film with a low dose of UV light, applying a photomask that allowed exposing selected areas with a higher dose of UV light (Figure S4c), and subsequent PEB (130 °C, 60 min) and developing. Based on the data shown in Figure 1, the different zones can be expected to exhibit the same dry modulus of E' = 1.8 GPa, whereas in ACSF at 37 °C E' values of 13 and 1330 MPa (at 37 °C) are expected for creases and panels, respectively. Indeed, after swelling in ACSF, the object retains its resistance to folding against the creases (Figure 2a) whereas it can be easily folded in the direction parallel to the creases (Figure 2b).

In order to facilitate rapid prototyping and produce more sophisticated structures, we explored the possibility to process the photoresist by direct writing (DW) using a maskless aligner.[39,40] Thus, 150−250 μm thick films were prepared by solvent casting the photoresist onto a flat support. The PAG content in the photoresist was increased to 2.0% w/w to accommodate for the long writing time of DW (all DW experiments were carried out with exposure at 365 nm) and thus reduce the overall process duration while keeping the influence of optical gradients and consequently of cross-linking gradients at a negligible level. The outcome of UV irradiation to the same nominal dose in different exposure systems varies substantially, on account of optical (spectral bandwidth, focus of the beam, reflectivity of the film substrate) and thermal (light-induced heating of the photoresist, temperature control) parameters.[41] We therefore carried out a series of DW experiments with wafer-supported films, different irradiation doses, PEB of 30 min at 130 °C, and standard developing. Swelling experiments and DMA data of the samples thus made show that similar property combinations as presented in Figure 1 are accessible (Figures S7 and S8), although the nominal exposure doses differ. We used the DW process to fabricate a functionally graded film with a pattern of alternating angled stripes created by low (6000 mJ/cm^2) and high (16 000 mJ/cm^2) doses, mirroring the design of reported bending actuators (Figure S9).[42,43] Figure 2c and d shows that the object indeed bends after exposure to emulated physiological conditions, as expected on the basis of inhomogeneous swelling. The possibility to preprogram actuation into a mechanically adaptive polymer by a simple DW process should be useful to impart cortical devices with active deployment options that are activated post implantation or for self-wrapping electrode−nerve interfaces for peripheral nervous system applications.[44]

https://doi.org/10.1021/acspolymersau.1c00037
ACS Polym. Au 2022, 2, 50−58

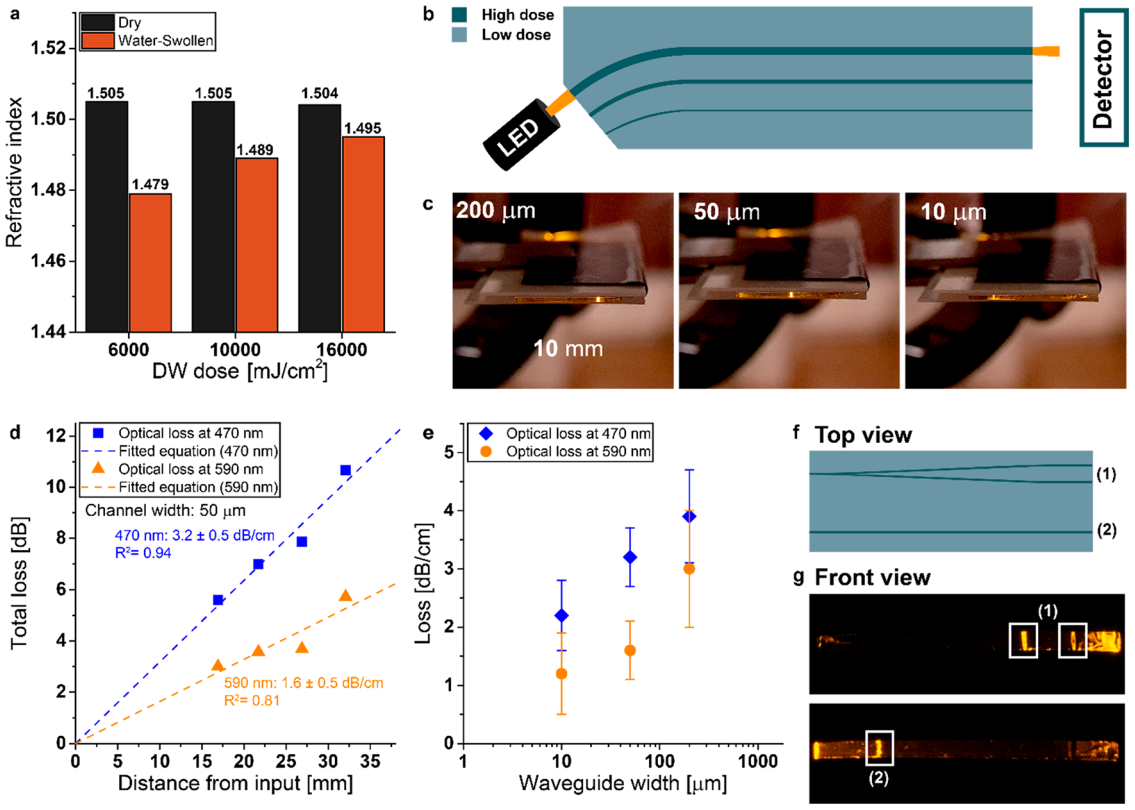

Figure 3. Fabrication of optical waveguides. (a) Refractive indices of the materials fabricated by direct writing at 20 °C in the dry and water-swollen state. (b) Structure of the optical waveguides produced and the setup used to study their properties. (c) Front view picture of the water-swollen device (structure as in (b)) sandwiched between PET sheets guiding 590 nm light through the 200 μm (left), 50 μm (middle), and 10 μm (right) wide channel. (d) Optical loss of the water-swollen 50 μm wide waveguide shown in (c) with 470 nm (blue) and 590 nm (amber) input light as a function of length. Dashed lines represent linear fits and the losses extracted from the slopes are indicated. (e) Optical loss of the water-swollen waveguides as a function of incident wavelength and channel diameter. (f) Design of a device with a splitter (1) and straight channel (2) waveguide. (g) Front view picture of the water-swollen splitter (top, (1)) and straight channel (bottom, (2)). Processing conditions: exposition with maskless aligner, 365 nm, 6000 mJ/cm^2 (light blue), 16 000 mJ/cm^2 (dark blue = high exposure dose). PEB: 130 °C, 30 min. All water-swollen samples were equilibrated in water at 25 °C for 2 h. Reported values in (a) and (d) are for n = 1 measurement. Reported values in (e) are the slope ± SD of a linear fit of 4 optical loss measurements at different channel lengths.

Of particular relevance in the context of implantable optical sensors and probes for optogenetics is that the adaptive polymer networks have a high transmittance in both the dry and the water-swollen state (>90% transmittance in the 400–800 nm range, Figure S10) and that the refractive index (RI) changes considerably upon aqueous swelling (since swelling experiments revealed no significant difference between ACSF and water and only a minor influence of the temperature, Figure S11, all optical experiments were carried out with samples that had been equilibrated in water for 2 h at room temperature). Films processed by DW and exposure doses of 6000, 10 000, or 16 000 mJ/cm^2, subsequent PEB at 130 °C for 30 min, and standard developing all exhibit the same RI of 1.505 in the dry state, as shown in Figure 3a. Upon absorption of water (RI = 1.333), the RI drops to 1.495–1.479 with a dose dependence (Figure 3a) that mirrors the swelling data (Figure S7c); that is, the material produced with the highest exposure dose exhibits the lowest degree of swelling and therefore the highest RI.

To explore if spatial control of the RI by DW would allow the photolithographic fabrication of mechanically adaptive objects with built-in optical waveguides, a waveguide featuring three channels with widths of 10, 50, and 200 μm was fabricated. Thus, the entire photoresist film was irradiated with a dose of 6000 mJ/cm^2 to fix the global shape and define the properties of the majority portions, before the waveguiding channels were written by exposing these areas with an additional dose of 10 000 mJ/cm^2 (PEB at 130 °C, 30 min, Figure S12). The channels were designed to feature bends (Figure 3b) in order to unequivocally confirm that light is indeed guided and not simply transmitted. After equilibrating the developed waveguide in water, the soft object was placed between two wetted poly(ethylene terephthalate) (PET) sheets that provided mechanical support. As seen in Figure 3c, light is clearly guided through the channels when the devices are equilibrated in water, confirming that the channels exhibit a higher cross-link density and RI than those of the water-swollen material surrounding them, so that the total internal reflection condition required for waveguiding is met.[45] We measured the optical losses of the water-swollen waveguides at 470 and 590 nm using the cut-back method (Figure 3d,e).[46] The optical losses thus determined are between 1 and 4 dB/cm, depending on the wavelength and channel width. The losses are higher at 470 nm, on account of increased scattering effects at the shorter wavelength. The fact that the losses also scale with the width of the channels is likely related to the fact that no cladding was applied to the exposed portions of the device so that the influence of surface-roughness-induced losses increases with the channel width.[47] Considering the short implant lengths used in optogenetics,

https://doi.org/10.1021/acspolymersau.1c00037
ACS Polym. Au 2022, 2, 50–58

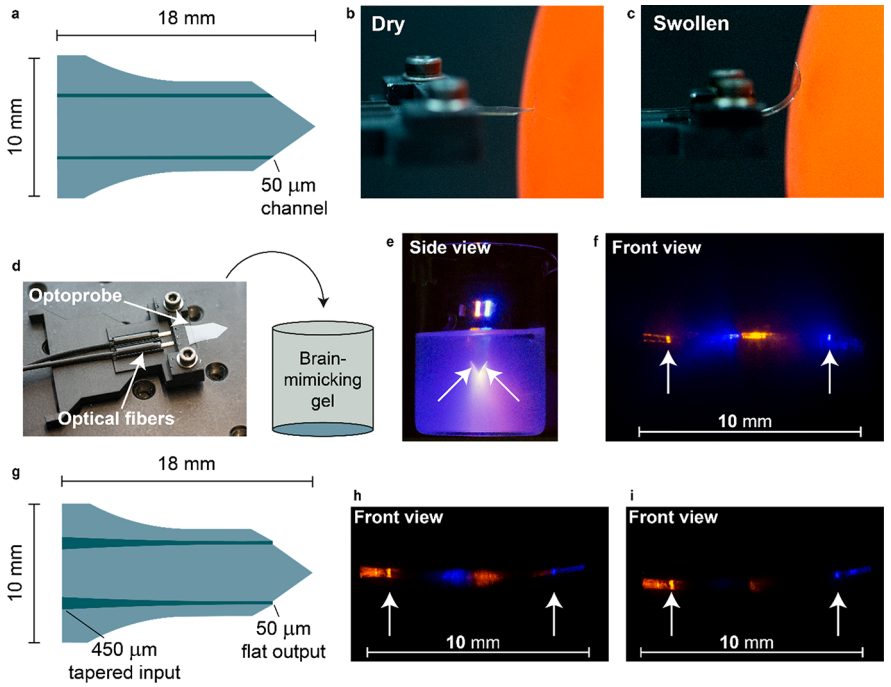

Figure 4. Fabrication of an optogenetic probe. (a) Design of the two-channel optoprobe. (b, c) Pictures of the dry (b) and water-swollen (c) optoprobe pushing on a soft object. (d) Picture of the two-channel optoprobe used for insertion experiments into a brain-mimicking gel. (e, f) Side (e) and front (f) view pictures of the optoprobe in the brain-mimicking gel. Arrows show the output locations of the waveguide channels. Water was added on top of the gel post implantation (not shown) to fully swell the part of the film that remains out of the gel (i.e., clamped on the support) and was removed prior to testing. (g) Design of the two-channel optoprobe with tapered waveguides. (h, i) Front view pictures of the optoprobe in the brain-mimicking gel without (h) and with (i) refractive-matching oil at the fiber-waveguide interface. Processing conditions: exposition with maskless aligner, 365 nm, 6000 mJ/cm^2 (light blue), 16 000 mJ/cm^2 (dark blue = high exposure dose). PEB: 130 °C, 30 min. All water-swollen samples were equilibrated in water at 25 °C for 2 h.

the optical losses of the present waveguides appear acceptable, but applying a cladding may prove useful to further improve the optical transmission of the waveguide, at the expanse of a more complicated multistep fabrication process. Alternatively, the waveguiding channels could be fabricated by two-photon lithography so that they are surrounded by a low-RI material. Circular or even free-form waveguides could also be manufactured using this approach.[48] To demonstrate that the process introduced here can be used to fabricate more complex waveguides, we produced a splitter/mixer device (Figure 3f), which represents an architecture that is commonly used in optogenetic probes.[11,30,49,50]

Gratifyingly, the splitting channel displays two outputs while the control (straight) channel shows only one output (Figure 3g). In the dry state, the RI is essentially the same throughout, and consequently, the light from a 590 nm LED source incoupled via an optical fiber is transmitted through the materials and not guided (Figure S14). We also fabricated a simple optogenetic probe featuring two straight channels (Figure 4a). The probe and two optical fibers (connected to 470 and 590 nm LED sources) were connected with a 3D-printed coupling support, as shown in Figure 4d. The dry probe easily penetrates an agar gel, which was used to mimic the mechanical properties of the brain, without buckling and then softens upon the absorption of water.[27,51] The softening can be visualized by pressing the optoprobe against a soft object. The dry optoprobe deforms the object (Figure 4b), whereas it bends when swollen (Figure 4c). DMA experiments on the optoprobe confirm the softening (Figure S15). After insertion into the brain-mimicking gel and equilibrium swelling, the front view of the probe, observed from the bottom of the gel (Figure 4j), clearly reveals the orange (590 nm) and blue (470 nm) light guided through the two channels, together with light that is transmitted through the probe and emitted from the tip, as the diameter of the optical fibers (220 μm) used to incouple the light was larger than the channel width (50 μm). A second probe featuring tapered channels (input width = 450 μm, output width = 50 μm, tapering angle = 1°) and flat outputs was fabricated and tested as described above. The intensity of light emanating from the tip is significantly reduced by the tapered design (Figure 4h) and almost completely eliminated by adding refractive matching oil (RI = 1.49) at the fiber−waveguide interface (Figure 4i). These results highlight the need for efficient coupling to eliminate stray light and artifacts.

CONCLUSION

In summary, we have exploited a negative photoresist approach to photolithographically convert a HEMA-based copolymer into complex structures with locally tunable, physiologically responsive properties. Spatial control of the cross-linking density can easily be achieved via the exposure and postexposure bake conditions, and this allows tuning of the water take-up, mechanical characteristics, as well as the refractive index of these materials in the water-swollen state. The simple demonstrators fabricated in our study demonstrate that it is possible to use the approach to create adaptive devices that offer, without any optimization, optical and mechanical properties that appear to be useful for optogenetics and other applications. The examples show that the shape and dimensions of the devices can be readily altered and that

https://doi.org/10.1021/acspolymersau.1c00037
ACS Polym. Au 2022, 2, 50−58

controlling their properties in a spatially resolved manner is straightforward. Reducing the size and increasing the complexity of the devices should thus be readily possible. We further speculate that the optical losses can be further reduced by application of cladding layers or fabrication processes that employ two-photon lithography and which would allow the fabrication of circular or free-form waveguides that are surrounded by low-refractive index materials.

METHODS

Materials

2-Hydroxyethyl methacrylate (HEMA, >99%, Sigma-Aldrich), 2-hydroxyethyl acrylate (HEA, 96%, Sigma-Aldrich), 2-ethylhexyl methacrylate (EHMA, >99%, TCI), 2,2′-azobis(2-methylpropionitrile) (AIBN, >98%, Sigma-Aldrich), dodecanethiol (99%, Sigma-Aldrich), hydroquinone (>99%, Fluka), (4-phenylthiophenyl)-diphenylsulfonium triflate (Sigma-Aldrich), potassium chloride (anhydrous, >99%, Sigma-Aldrich), sodium phosphate monobasic monohydrate (>99%, Sigma-Aldrich), sodium phosphate dibasic heptahydrate (98−102%, Sigma-Aldrich), calcium chloride dihydrate (>99%, Sigma-Aldrich), magnesium chloride hexahydrate (99−102%, Sigma-Aldrich), sodium chloride (>99%, Sigma-Aldrich), and refractive-matching oil (RI = 1.49, Cargille) were used without further purification, except for AIBN, which was recrystallized twice from methanol. ACSF was prepared as reported elsewhere.[52] p(HEMA-*co*-HEA-*co*-EHMA) was synthesized according to a known procedure.[27] The composition of the polymer according to NMR was HEMA 57%, HEA 27%, and EHMA 16%. Photomasks were purchased from Selba S.A.

General Methods

All UV-sensitive substances (photoresist solutions and films) were stored and manipulated in a UV-free environment (using Lithoprotect Y520 UV-protection foils). Metal evaporation and DW experiments were performed in a Class 5 clean room.

ACSF was replaced by water for all optical measurements to avoid scattering issues caused by insoluble salt particles. Previous experiments on mechanically adaptive polymers demonstrated no significant difference between water-swollen and ACSF-swollen samples.[26]

Dynamic Mechanical Analyses

DMA experiments were performed on a TA Instruments Q800 DMA using a frequency strain analysis temperature ramp (0−180 °C, 3 °C/min, 8 min equilibration time at 0 °C) or an isothermal step (120 °C, 6 h) at an amplitude of 15 μm and a frequency of 1 Hz). Submersion DMA in ACSF was performed on the same instrument using a multifrequency strain analysis temperature ramp (5−75 °C, 3 °C/min) with an amplitude of 30 μm and a frequency of 1 Hz. Before submersion experiments, samples were conditioned by immersion in ACSF at 37 °C for 24 h. All DMA data reported are averages and standard deviation from triplicate measurements and the graphs presented show representative experiments.

Swelling

Precisely weighed amounts (10−15 mg) of the dry film samples were immersed in ACSF or water (4−5 mL) for 24 h at 37 °C (or 25 °C, when indicated). The samples were then wiped dry with a paper tissue and immediately weighed. The extent of swelling was calculated using the following formula:

$$\text{extent of swelling} = \frac{m_S - m_D}{m_D} \times 100$$

where m_D is the dry sample mass and m_S is the swollen sample mass. Values quoted are averages of three samples. Swelling kinetics were established by measuring weights over the course of 24 h using the above procedure. Temperature dependence of the swelling was determined by heating pre-equilibrated samples (+ medium) at 37 °C overnight prior to measurement.

Preparation of Free-Standing Photoresist Films

p(HEMA-*co*-HEA-*co*-EHMA) (1.00 g) and 4-phenylthiophenyl)-diphenylsulfonium triflate (5 mg, 0.5 wt %) were dissolved in methanol (8 mL). The solution was stirred at room temperature until dissolution was complete. The solution was then filtered through a 0.45 μm disk filter and poured into a poly(tetrafluoroethylene) (PTFE) Petri dish (6 cm diameter). After letting most of the solvent evaporate during 24 h in a well-ventilated hood at room temperature, a photoresist film had formed that was removed from the mold and completely dried under vacuum (rt → 100 °C). The dry films were then reprocessed by compression-molding at 125 °C. Films with a thickness of between 100 and 250 μm were produced.

Preparation of Wafer-Supported Photoresist Films

Silicon wafers (diameter = 2 in., thickness = 500 ± 50 μm, 1-side polished, Dummy CZ-Si, Microchemicals GmbH) were sequentially coated with chromium (3 nm) and copper (60−75 nm) using a thermal evaporation process on a Moorfield Nanolab 080 system. p(HEMA-*co*-HEA-*co*-EHMA) (700 mg) and 4-phenylthiophenyl)-diphenylsulfonium triflate (14 mg, 2 wt %) were dissolved in ethanol (2.5 mL). The solution was stirred at room temperature until dissolution was complete. The solution was then filtered through a 1 μm disk filter and poured onto the copper-coated silicon wafer. A Petri dish (15 cm diameter) was placed upside down over the wafer to slow down the evaporation. After letting the solvent evaporate during the course of 48−72 h in a well-ventilated hood, the wafer was placed on a Sawatec HP-150 hot plate and progressively heated to 130 °C over the course of 3 h to dry the film. Films with a thickness of between 100 and 250 μm were produced.

Processing of Free-Standing Photoresist Films

Rectangular samples (25 × 5 mm^2) for DMA experiments were cut from the dry photoresist films at 70 °C (to prevent the film from shattering) and were then placed into a PTFE Petri dish and irradiated in a Hönle LED Cube 100 IC (365 nm, 350−4500 mJ/cm^2). The light intensity was measured using a Hönle UV Meter BASIC equipped with a FS VIS D1 probe. For the photopatterning experiments, free-standing films were irradiated through a quartz photomask in a Hönle LED Cube 100 IC (365 nm, 350−4500 mJ/cm^2).

The postexposure bake was then performed for 30−60 min in a preheated oven at 90−130 °C. The samples were then developed in a 4:1 v/v methanol:water mixture for 20 min at room temperature before they were transferred into methanol/water mixtures in which the ratio was gradually changed from 3:2 to 2:3 to 1:4 v/v. The gradual solvent change caused the probed to slowly deswell. Samples were left in each bath for 20 min. Finally, the samples were dried in an oven at 100 °C overnight (normal pressure).

Processing of Wafer-Supported Photoresist Films by Direct Writing (DW)

Wafer-supported films were patterned using a Heidelberg μMLA DW system (365 nm, fast mode, pneumatic autofocus, dose 6000−16 000 mJ/cm^2). The patterns were designed using the KLayout software. After the patterning step, the wafer was placed on a Sawatec HP-150 hot plate and a postexposure bake was performed (130 °C, 30 min). The wafer was then placed in a water/ethanol solution (4:1 v/v) for 24 h. Using a spatula, the developed film was carefully removed from the wafer and transferred into a water/ethanol mixture in which the ethanol content was gradually increased from 4:1 to 1:4 v/v to fully develop the patterned film. After 1 h in a 1:4 v/v water/ethanol mixture, water was gradually added to deswell the patterned film. Finally, the patterned film was dried in an oven at 100 °C overnight (normal pressure).

Waveguide Production Using Direct Writing (DW)

The waveguides were produced as follows: a wafer-supported film (thickness = 150−250 μm) was exposed using a Heidelberg μMLA system (365 nm, fast mode, pneumatic autofocus, dose 6000 mJ/cm^2) to define the overall shape of the object. Waveguiding channels with a width of 50−400 μm were then exposed on the patterned film with a

https://doi.org/10.1021/acspolymersau.1c00037
ACS Polym. Au 2022, 2, 50−58

dose of 10 000 mJ/cm^2 to obtain a total dose of 16 000 mJ/cm^2. The wafer-supported film was then processed according to the procedure described above.

Transmittance and Reflectance Measurements

A wafer-supported film (thickness = 300 μm) was exposed using a Heidelberg μMLA system (365 nm, fast mode, pneumatic autofocus, dose 6000 mJ/cm^2). The wafer-supported film was then processed according to the procedure described above. Transmittance and reflectance spectra of the film in the dry and water-swollen (swelling in deionized water at 25 °C for 2 h prior to measurement) were conducted using a Avasphere-50 integrated sphere (Avantes, The Netherlands) coupled to a spectrometer (FLAME-T-XR1-ES, Ocean Optics, United States). The sample was illuminated by a xenon light source (Ocean Optics HPX-2000). For reflection, a white diffuse standard was used as a reference.

Refractive Index Measurements

A wafer-supported photoresist film (thickness = 150−250 μm) was exposed using a Heidelberg μMLA system (365 nm, fast mode, pneumatic autofocus, dose 6000, 10 000, and 16 000 mJ/cm^2) and processed according to the procedure described above to obtain 1 cm × 1 cm square samples. The refractive index of the samples in the dry state and after being immersed in deionized water for 1 h was measured using a Kern Optics Abbe refractometer at 20 °C.

Optical Loss Measurements

A film with waveguiding channels (film thickness = 150−250 μm, channel width= 50, 200, and 400 μm) was placed in deionized water for 24 h prior to the measurement. The swollen film was then placed between two PET support sheets, and water was added to act as cladding and prevent the drying of the waveguide. A blue (470 nm, M470F1, 10.1 mW, ThorLabs) or orange (590 nm, M590F1, 3.2 mW, ThorLabs) fiber-coupled high-power LED was aligned to the waveguide, and the optical losses were determined by the cutback method using a photodiode (S120VC, ThorLabs) coupled with a photometer (PM100USB, ThorLabs). Optical losses were determined by a linear fit of the measured intensity at four different channel lengths.

■ ASSOCIATED CONTENT

Supporting Information

The Supporting Information is available free of charge at https://pubs.acs.org/doi/10.1021/acspolymersau.1c00037.

DMA curves of the materials, schemes of the fabrication process, schemes of the photomask and lithographic designs, optical properties of the materials (PDF)

■ AUTHOR INFORMATION

Corresponding Author

Christoph Weder − *Adolphe Merkle Institute, University of Fribourg, CH-1700 Fribourg, Switzerland;* orcid.org/0000-0001-7183-1790; Email: christoph.weder@unifr.ch

Authors

Baptiste Monney − *Adolphe Merkle Institute, University of Fribourg, CH-1700 Fribourg, Switzerland;* orcid.org/0000-0003-4212-1284

Cédric Kilchoer − *Adolphe Merkle Institute, University of Fribourg, CH-1700 Fribourg, Switzerland*

Complete contact information is available at: https://pubs.acs.org/10.1021/acspolymersau.1c00037

Author Contributions

B.M. and C.W. conceived the idea and designed the study. B.M. synthesized and characterized the materials and developed the photolithography procedure. B.M. and C.K. designed the waveguides and measured their optical properties. All authors discussed the results and wrote the paper.

Funding

The authors are grateful for the financial support received from the Swiss National Science Foundation (Grant No. 200020_172619 and IZPIP0_177995), the NCCR Bioinspired Materials, (Grant No. 51NF40-182881) and the Adolphe Merkle Foundation.

Notes

The authors declare the following competing financial interest(s): The employer of the authors has been granted a patent that protects physiologically responsive mechanically adaptive polymer optical fibers (Weder, C.; Jorfi, M.; Foster, E.J.; Physiologically Responsive Mechanically Adaptive Polymer Optical Fibers, Production and Methods of Use; US Patent 10,481,323 (2019).

The data sets will be made available through the Zenodo Sharing platform.

■ ACKNOWLEDGMENTS

The authors would like to thank Dr. Allison E. Hess-Dunning and Dr. Esteban Bermúdez-Ureña for their advice concerning the photolithography experiments.

■ REFERENCES

(1) Montero De Espinosa, L.; Meesorn, W.; Moatsou, D.; Weder, C. Bioinspired Polymer Systems with Stimuli-Responsive Mechanical Properties. *Chem. Rev.* **2017**, *117* (20), 12851−12892.

(2) Park, Y.; Chen, X. Water-Responsive Materials for Sustainable Energy Applications. *J. Mater. Chem. A* **2020**, *8* (31), 15227−15244.

(3) Ma, M.; Guo, L.; Anderson, D. G.; Langer, R. Bio-Inspired Polymer Composite Actuator and Generator Driven by Water Gradients. *Science* **2013**, *339* (6116), 186−189.

(4) Kunzelman, J.; Crenshaw, B. R.; Weder, C. Self-Assembly of Chromogenic Dyes—a New Mechanism for Humidity Sensors. *J. Mater. Chem.* **2007**, *17* (29), 2989−2991.

(5) Kamtsikakis, A.; Baales, J.; Zeisler-Diehl, V. V.; Vanhecke, D.; Zoppe, J. O.; Schreiber, L.; Weder, C. Asymmetric Water Transport in Dense Leaf Cuticles and Cuticle-Inspired Compositionally Graded Membranes. *Nat. Commun.* **2021**, *12* (1), 1267.

(6) Zhang, J., Ed. *Switchable and Responsive Surfaces and Materials for Biomedical Applications*; Elsevier, 2015.

(7) McMillan, S.; Rader, C.; Jorfi, M.; Pickrell, G.; Foster, E. J. Mechanically Switchable Polymer Fibers for Sensing in Biological Conditions. *J. Biomed. Opt.* **2017**, *22* (2), 027001.

(8) Park, S.; Yuk, H.; Zhao, R.; Yim, Y. S.; Woldeghebriel, E. W.; Kang, J.; Canales, A.; Fink, Y.; Choi, G. B.; Zhao, X.; Anikeeva, P. Adaptive and Multifunctional Hydrogel Hybrid Probes for Long-Term Sensing and Modulation of Neural Activity. *Nat. Commun.* **2021**, *12* (1), 3435.

(9) Tang, C.; Xie, S.; Wang, M.; Feng, J.; Han, Z.; Wu, X.; Wang, L.; Chen, C.; Wang, J.; Jiang, L.; Chen, P.; Sun, X.; Peng, H. A Fiber-Shaped Neural Probe with Alterable Elastic Moduli for Direct Implantation and Stable Electronic−Brain Interfaces. *J. Mater. Chem. B* **2020**, *8* (20), 4387−4394.

(10) Lebedev, M. A.; Nicolelis, M. A. L. Brain-Machine Interfaces: From Basic Science to Neuroprostheses and Neurorehabilitation. *Physiol. Rev.* **2017**, *97* (2), 767−837.

(11) Alt, M. T.; Fiedler, E.; Rudmann, L.; Ordonez, J. S.; Ruther, P.; Stieglitz, T. Let There Be Light—Optoprobes for Neural Implants. *Proc. IEEE* **2017**, *105* (1), 101−138.

(12) Bouton, C. E.; Shaikhouni, A.; Annetta, N. V.; Bockbrader, M. A.; Friedenberg, D. A.; Nielson, D. M.; Sharma, G.; Sederberg, P. B.; Glenn, B. C.; Mysiw, W. J.; Morgan, A. G.; Deogaonkar, M.; Rezai, A.

R. Restoring Cortical Control of Functional Movement in a Human with Quadriplegia. *Nature* **2016**, *533* (7602), 247−250.
(13) Chen, X.; Wang, F.; Fernandez, E.; Roelfsema, P. R. Shape Perception via a High-Channel-Count Neuroprosthesis in Monkey Visual Cortex. *Science* **2020**, *370* (6521), 1191−1196.
(14) McGlynn, E.; Nabaei, V.; Ren, E.; Galeote-Checa, G.; Das, R.; Curia, G.; Heidari, H. The Future of Neuroscience: Flexible and Wireless Implantable Neural Electronics. *Adv. Sci.* **2021**, *8* (10), 2002693.
(15) Delbeke, J.; Hoffman, L.; Mols, K.; Braeken, D.; Prodanov, D. And Then There Was Light: Perspectives of Optogenetics for Deep Brain Stimulation and Neuromodulation. *Front. Neurosci.* **2017**, *11*, 663.
(16) Rajasethupathy, P.; Ferenczi, E.; Deisseroth, K. Targeting Neural Circuits. *Cell* **2016**, *165* (3), 524−534.
(17) Lacour, S. P.; Courtine, G.; Guck, J. Materials and Technologies for Soft Implantable Neuroprostheses. *Nat. Rev. Mater.* **2016**, *1* (10), 16063.
(18) Jorfi, M.; Skousen, J. L.; Weder, C.; Capadona, J. R. Progress towards Biocompatible Intracortical Microelectrodes for Neural Interfacing Applications. *J. Neural Eng.* **2015**, *12* (1), 011001.
(19) Salatino, J. W.; Ludwig, K. A.; Kozai, T. D. Y.; Purcell, E. K. Glial Responses to Implanted Electrodes in the Brain. *Nat. Biomed. Eng.* **2017**, *1* (11), 862−877.
(20) Sridharan, A.; Nguyen, J. K.; Capadona, J. R.; Muthuswamy, J. Compliant Intracortical Implants Reduce Strains and Strain Rates in Brain Tissue in Vivo. *J. Neural Eng.* **2015**, *12* (3), 036002.
(21) Lecomte, A.; Descamps, E.; Bergaud, C. A Review on Mechanical Considerations for Chronically-Implanted Neural Probes. *J. Neural Eng.* **2018**, *15* (3), 031001.
(22) Lee, H. C.; Ejserholm, F.; Gaire, J.; Currlin, S.; Schouenborg, J.; Wallman, L.; Bengtsson, M.; Park, K.; Otto, K. J. Histological Evaluation of Flexible Neural Implants; Flexibility Limit for Reducing the Tissue Response? *J. Neural Eng.* **2017**, *14* (3), 036026.
(23) Capadona, J. R.; Tyler, D. J.; Zorman, C. A.; Rowan, S. J.; Weder, C. Mechanically Adaptive Nanocomposites for Neural Interfacing. *MRS Bull.* **2012**, *37* (6), 581−589.
(24) Ware, T.; Simon, D.; Liu, C.; Musa, T.; Vasudevan, S.; Sloan, A.; Keefer, E. W.; Rennaker, R. L.; Voit, W. Thiol-Ene/Acrylate Substrates for Softening Intracortical Electrodes. *J. Biomed. Mater. Res., Part B* **2014**, *102B* (1), 1−11.
(25) Capadona, J. R.; Shanmuganathan, K.; Tyler, D. J.; Rowan, S. J.; Weder, C. Stimuli-Responsive Polymer Nanocomposites Inspired by the Sea Cucumber Dermis. *Science* **2008**, *319* (5868), 1370−1374.
(26) Monney, B.; Dibble, A. G.; Moatsou, D.; Weder, C. Highly Cross-Linked, Physiologically Responsive, Mechanically Adaptive Polymer Networks Made by Photopolymerization. *ACS Omega* **2020**, *5* (6), 3090−3097.
(27) Monney, B.; Hess-Dunning, A. E.; Gloth, P.; Capadona, J. R.; Weder, C. Mechanically Adaptive Implants Fabricated with Poly(2-Hydroxyethyl Methacrylate)-Based Negative Photoresists. *J. Mater. Chem. B* **2020**, *8* (30), 6357−6365.
(28) Ware, T.; Simon, D.; Arreaga-Salas, D. E.; Reeder, J.; Rennaker, R.; Keefer, E. W.; Voit, W. Fabrication of Responsive, Softening Neural Interfaces. *Adv. Funct. Mater.* **2012**, *22* (16), 3470−3479.
(29) Jorfi, M.; Voirin, G.; Foster, E. J.; Weder, C. Physiologically Responsive, Mechanically Adaptive Polymer Optical Fibers for Optogenetics. *Opt. Lett.* **2014**, *39* (10), 2872−2875.
(30) Son, Y.; Jenny Lee, H.; Kim, J.; Shin, H.; Choi, N.; Justin Lee, C.; Yoon, E.-S.; Yoon, E.; Wise, K. D.; Geun Kim, T.; Cho, I.-J. In Vivo Optical Modulation of Neural Signals Using Monolithically Integrated Two-Dimensional Neural Probe Arrays. *Sci. Rep.* **2015**, *5* (1), 15466.
(31) Im, M.; Cho, I. J.; Wu, F.; Wise, K. D.; Yoon, E. Neural Probes Integrated with Optical Mixer/Splitter Waveguides and Multiple Stimulation Sites. *Proc. IEEE Int. Conf. Micro Electro Mech. Syst.* **2011**, 1051−1054.
(32) Aoai, T.; Lee, J. S.; Watanabe, H.; Kondo, S.; Miyagawa, N.; Takahara, S.; Yamaoka, T. Mechanism of Acid-Catalyzed Crosslinking Reaction with Hydroxyethyl Group and Application to Microlithography. *J. Photopolym. Sci. Technol.* **1999**, *12* (2), 303−306.
(33) Vasilopoulou, M.; Boyatzis, S.; Raptis, I.; Dimotikalli, D.; Argitis, P. Evaluation of Poly(Hydroxyethyl Methacrylate) Imaging Chemistries for Micropatterning Applications. *J. Mater. Chem.* **2004**, *14* (22), 3312−3320.
(34) Diakoumakos, C. D.; Raptis, I.; Tserepi, A.; Argitis, P. Free-Radical Synthesis of Narrow Polydispersed 2-Hydroxyethyl Methacrylate-Based Tetrapolymers for Dilute Aqueous Base Developable Negative Photoresists. *Polymer* **2002**, *43* (4), 1103−1113.
(35) Lee, J.; Aoai, T.; Kondo, S. N. I.; Miyagawa, N.; Takahara, S.; Yamaoka, T. Negative-Working Photoresist of Methacrylate Polymers Based on the Transesterification of the 2-Hydroxyethyl Group in the Presence of an Acid. *J. Polym. Sci., Part A: Polym. Chem.* **2002**, *40* (11), 1858−1867.
(36) Oleinik, E. F. Epoxy-Aromatic Amine Networks in the Glassy State Structure and Properties. In *Epoxy Resins and Composites IV. Advances in Polymer Science*; Dušek, K., Ed.; Springer: Berlin, Heidelberg, 1986; Vol. *80*, pp 49−99.
(37) Miserez, A.; Schneberk, T.; Sun, C.; Zok, F. W.; Waite, J. H. The Transition from Stiff to Compliant Materials in Squid Beaks. *Science* **2008**, *319* (5871), 1816−1819.
(38) Eder, M.; Amini, S.; Fratzl, P. Biological Composites—Complex Structures for Functional Diversity. *Science* **2018**, *362* (6414), 543−547.
(39) Gittard, S. D.; Narayan, R. J. Laser Direct Writing of Micro- and Nano-Scale Medical Devices. *Expert Rev. Med. Devices* **2010**, *7* (3), 343−356.
(40) Scholten, K.; Meng, E. Materials for Microfabricated Implantable Devices: A Review. *Lab Chip* **2015**, *15* (22), 4256−4272.
(41) Rinke, T.; Koch, C. *Photolithography: Basics of Microstructuring*, 2nd ed.; MicroChemicals GmbH: Ulm, 2017.
(42) Wu, Z. L.; Moshe, M.; Greener, J.; Therien-Aubin, H.; Nie, Z.; Sharon, E.; Kumacheva, E. Three-Dimensional Shape Transformations of Hydrogel Sheets Induced by Small-Scale Modulation of Internal Stresses. *Nat. Commun.* **2013**, *4* (1), 1586.
(43) Zhang, Y.; Pon, N.; Awaji, A.; Rowan, S. J. Squid Beak Inspired Cross-Linked Cellulose Nanocrystal Composites. *Biomacromolecules* **2021**, *22* (1), 201−212.
(44) Zhang, Y.; Zheng, N.; Cao, Y.; Wang, F.; Wang, P.; Ma, Y.; Lu, B.; Hou, G.; Fang, Z.; Liang, Z.; Yue, M.; Li, Y.; Chen, Y.; Fu, J.; Wu, J.; Xie, T.; Feng, X. Climbing-Inspired Twining Electrodes Using Shape Memory for Peripheral Nerve Stimulation and Recording. *Sci. Adv.* **2019**, *5* (4), eaaw1066.
(45) Okamoto, K. *Fundamentals of Optical Waveguides*; Elsevier, 2006.
(46) Reed, G. T. Methods of Measurement of Passive Integrated Optical Waveguides. *IEE Colloquium on Measurements on Optical Devices*; 1992; pp 2/1−2/7.
(47) Li, Y. P.; Henry, C. H. Silicon Optical Bench Waveguide Technology. In *Optical Fiber Telecommunications IIIB*; Kaminow, I. P., Koch, T. L., Eds.; Elsevier, 1997; pp 319−376.
(48) Malinauskas, M.; Farsari, M.; Piskarskas, A.; Juodkazis, S. Ultrafast Laser Nanostructuring of Photopolymers: A Decade of Advances. *Phys. Rep.* **2013**, *533* (1), 1−31.
(49) Kampasi, K.; English, D. F.; Seymour, J.; Stark, E.; McKenzie, S.; Vöröslakos, M.; Buzsáki, G.; Wise, K. D.; Yoon, E. Dual Color Optogenetic Control of Neural Populations Using Low-Noise, Multishank Optoelectrodes. *Microsystems Nanoeng.* **2018**, *4* (1), 10.
(50) Im, M.; Cho, I.-J.; Wu, F.; Wise, K. D.; Yoon, E. Neural Probes Integrated with Optical Mixer/Splitter Waveguides and Multiple Stimulation Sites. *2011 IEEE 24th International Conference on Micro Electro Mechanical Systems* **2011**, 1051−1054.
(51) Chen, Z.-J.; Gillies, G. T.; Broaddus, W. C.; Prabhu, S. S.; Fillmore, H.; Mitchell, R. M.; Corwin, F. D.; Fatouros, P. P. A Realistic Brain Tissue Phantom for Intraparenchymal Infusion Studies. *J. Neurosurg.* **2004**, *101* (2), 314−322.

https://doi.org/10.1021/acspolymersau.1c00037
ACS Polym. Au 2022, 2, 50−58

(52) Preparation of Artificial CSF. *ALZET Osmotic Pumps*. https://www.alzet.com/guide-to-use/preparation-of-artificial-csf/ (accessed 2021-04-16).

https://doi.org/10.1021/acspolymersau.1c00037
ACS Polym. Au 2022, 2, 50−58